ACS APPLIED MATERIALS & INTERFACES

Research Article

www.acsami.org

High Electrochemical Performances of Microsphere C-TiO_2 Anode for Sodium-Ion Battery

Seung-Min Oh,[†] Jang-Yeon Hwang,[†] C. S. Yoon,[‡] Jun Lu,[§] Khalil Amine,[§] Illias Belharouak,[§,∥] and Yang-Kook Sun*,[†]

[†]Department of Energy Engineering and [‡]Department of Materials Science and Engineering, Hanyang University, Seoul 133-791, Republic of Korea

[§]Chemical Sciences and Engineering Division, Argonne National Laboratory, 9700 South Cass Avenue, Lemont, Illinois 60439, United States

[∥]Qatar Environment & Energy Research Institute, Qatar Foundation, P.O. Box 5825, Doha, Qatar

Supporting Information

ABSTRACT: High-power, long-life carbon-coated TiO_2 microsphere electrodes were synthesized by a hydrothermal method for sodium ion batteries, and the electrochemical properties were evaluated as a function of carbon content. The carbon coating, introduced by sucrose addition, had an effect of suppressing the growth of the TiO_2 primary crystallites during calcination. The carbon coated TiO_2 (sucrose 20 wt % coated) electrode exhibited excellent cycle retention during 50 cycles (100%) and superior rate capability up to a 30 *C* rate at room temperature. This cell delivered a high discharge capacity of 155 mAh $g_{composite}^{-1}$ at 0.1 *C*, 149 mAh $g_{composite}^{-1}$ at 1 *C*, and 82.7 mAh $g_{composite}^{-1}$ at a 10 *C* rate, respectively.

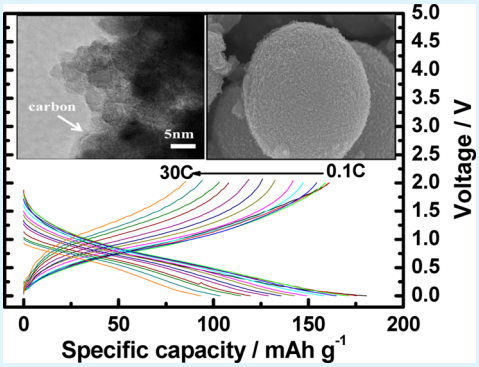

KEYWORDS: *hydrothermal method, anode, TiO_2, Na battery, carbon coating*

INTRODUCTION

The demand for renewable energy storage devices has greatly increased, especially for potential use in electric vehicles and energy storage systems. For this reason, lithium-ion batteries have been widely studied and their performance has been much improved during the past two decades. However, several problems with lithium-ion batteries still remain, including their rising costs and limited natural sources of lithium.[1,2] Consequently, many researchers are shifting their focus to sodium-ion based batteries because of their lower costs and the abundance of sodium sources.[3−11]

Many types of commercial batteries use carbonaceous materials for the anode, such as meso-carbon microbeads (MCMB) or hard carbon. However, MCMB cannot be used as an anode material for sodium batteries because of the high potential of the Na/Na^+ (~0.3 V higher than Li/Li^+) redox reaction and the large ionic radii of the Na^+ (102 pm).[3,4] Therefore, there have been many efforts to find a suitable anode material for the sodium-ion battery system. In the case of insertion anodes, various types of nongraphitic carbon materials have been considered and tested.[5−8] For example, Stevens and Dahn reported disordered carbon which has a discharge capacity of 300 mAh g^{-1},[5] but this material showed low cycle retention. To solve this problem, Komaba and Tirado changed the electrolyte to ameliorate the cyclability. However, the important issues of rate capability and energy density still remained to be resolved.[7,8]

Another types of anode materials which operated by insertion reaction were studied.[9−13] Among them, low potential $Na_2Ti_3O_7$ insertion material was reported by A. Rudola,[9] and Tarascon group.[10] These electrodes were able to sustain a capacity of about 180 mAh g^{-1} at *C*/10 and 200 mAh g^{-1} at *C*/25, but still need to improve the other electrochemical properties such as rate capability and cycle performance. Yamaki et al.[11] synthesized $NaTi_2(PO_4)_3$, which delivered 120 mAh g^{-1}. Meanwhile, Komaba et al.[12] synthesized Fe_3O_4-based anodes, which gave a discharge capacity of 150 mAh g^{-1}. However, these materials also have drawbacks, such as low cycle retention (Fe_3O_4), a higher potential window (Fe_3O_4, $NaTi_2(PO_4)_3$), and low discharge capacity ($NaTi_2(PO_4)_3$). Also, these materials have nanosized morphologies, which exhibited the low energy density and first cycle efficiency. Recently, nanocrystalline anatase TiO_2 materials were tested for Na-ion batteries; they were synthesized via cellulose-based paper template method or purchased from Sigma-Aldrich company.[13,14] Nanocrystalline TiO_2 material delivered a discharge capacity of about 150 mAh g^{-1} with reasonable

Received: March 24, 2014
Accepted: June 20, 2014
Published: June 20, 2014

cycle performance. And, self-organized titania nanotubes were prepared via anodization method which reported by Gonzalez et al.[15] This TiO_2 nanotube electrode delivered a capacity of about 200 mAh g^{-1} at 0.1 mA cm^{-2}. However, these materials show a poor rate capability. To enhance the electrochemical performance, K.-T. Kim et al. introduced carbon-coated TiO_2 nanorods material, which show stable cycle retention with good rate capability.[16] However, it still has the important problem of low energy density, which is caused by low tap density of nanorods material.

From the results of our previous experiments, it was confirmed that the non-carbon-coated anatase-type microsphere TiO_2 anode material has several advantages for the lithium-ion battery system, including excellent cycle retention, high efficiency, good rate capability, and high energy density.[17] In this paper, we therefore introduce the carbon-coated TiO_2 microsphere synthesized by a hydrothermal method as an anode for the sodium-ion battery system. For this study, physical and electrochemical properties of the electrode were evaluated as a function of carbon amounts.

EXPERIMENTAL SECTION

Material Synthesis. The mesoporous anatase-phase TiO_2 sphere was synthesized by a hydrothermal method, as previously reported,[17] in which $TiCl_4$ was used as the starting material. A required amount of high-purity $TiCl_4$ was added dropwise to a distilled water−ethanol mixture in ice to make the $TiOCl_2$ solution. A calculated quantity of urea was then added to the $TiOCl_2$ solution with continuous stirring. The urea was added to control the rate of hydrolysis, whereby the ammonia produced by the hydrolysis of urea controls the pH of the reaction at a temperature greater than 80 °C. A calculated quantity of ammonium sulfate was added to the clear solution obtained after the addition of urea, and this solution was stirred for 4 h. The resultant transparent solution was transferred to a Teflon-sealed autoclave and heated at a temperature of 120 °C for 24 h. After the reaction was completed, the autoclave was cooled to room temperature, and the resultant slurry was filtered and washed three times with absolute ethanol. The powder (non-carbon-coated sample) was obtained by drying the washed slurry in vacuum oven at 60 °C, and then sintering it at 400 °C for 5 h in an Ar gas atmosphere. To obtain the carbon-coated TiO_2 powders, 2 g of as-synthesized TiO_2 powder and the required amount of sucrose (10−40 wt %) were poured into 20 mL of water and stirred at 80 °C until the water dried. It was then dried in vacuum oven at 60 °C for 5 h and calcined at 400 °C for 5 h in an Ar gas atmosphere.

Physical and Chemical Characterization. The synthesized materials of the crystalline phase were characterized by powder X-ray diffraction (XRD, Rint-2000, Rigaku, Japan) measurements using Cu−Kα radiation. Particle morphologies of the precursor and the as-synthesized powders were observed by scanning electron microscopy (SEM, JSM 6400, JEOL Ltd., Japan) and transmission electron microscopy (TEM, JEOL, 2010). An elemental analyzer (EA110, CE Instrument) and thermogravimetric analyzer (loaded sample amount 10 mg, TG 209, Netzsch, Germany), were employed to determine the amount of carbon in the final products. The conductivity of disc-shaped pellets (diameter 20 mm, thickness 4.0 mm, weight 1.5 g) of the synthesized material was measured using a four-point DC method at 25 °C. X-ray photoelectron spectroscopy (XPS, PHI 5600, PerkinElmer, USA) measurements were performed to obtain information on the oxidation state values of transition metals. Macro-mode (about 3 mm × 3 mm) Ar-ion etching was used to examine the concentration depth profiles of the coated powders. The etching rate was estimated to be 5 Å min^{-1} for silica. Crystallite sizes of the each TiO_2 powder was calculated from the major diffraction peaks of TiO_2 using Scherrer's equation ($D_c = K\lambda/(\theta_{1/2}/\cos\theta_B)$), where K is a constant (ca. 0.9), λ is the X-ray wavelength (1.5418 Å), θ_B is the Bragg angle at the highest peak point, and $\theta_{1/2}$ is the pure diffraction broadening of a peak at half-height, that is, the full-width at half-maximum depends only on the crystallite dimension. The surface area and porosity of each TiO_2 material were determined by using a Quantachrome Autosorb-iQ-MP automated gas adsorption system using nitrogen as the adsorbate at a temperature of 77 K. The specific surface area was calculated using the Brunauer−Emmett−Teller (BET) method, and the pore diameters were obtained from the adsorption branch of the isotherm using the Barrett−Joyner−Halenda (BJH) method.

Electrochemical Characterization. Electrochemical testing was performed in an R2032 coin-type cell adopting Na metal (Alfa Aesar, USA) as an anode. The cathodes were fabricated by blending the prepared TiO_2 powders (80 wt %), carbon black (10 wt %), and polyvinylidene fluoride (10 wt %) in *N*-methylpyrrolidinon. The slurry was then cast on copper foil and dried at 110 °C for 12 h in a vacuum oven, and then disks were punched out of the foil. The loading amount of active material on the whole electrodes is 4.0 mg cm^{-2}. The electrolyte solution used was 1.0 M $NaClO_4$ in a 98:2 volumetric mixture of propylene carbonate and fluoroethylene carbonate (PANAX ETEC Co., Ltd., Korea). All cells were prepared in an Ar-filled drybox. The cell was cycled in a constant current mode at a 0.1 *C* rate within a voltage range of 0.01−2.0 versus Na (where 1*C* = 200 mAh g^{-1}).

RESULTS AND DISCUSSION

Figure 1 shows the XRD patterns of the mesoporous micro-TiO_2 powders calcined at 400 °C for 5 h with different amounts

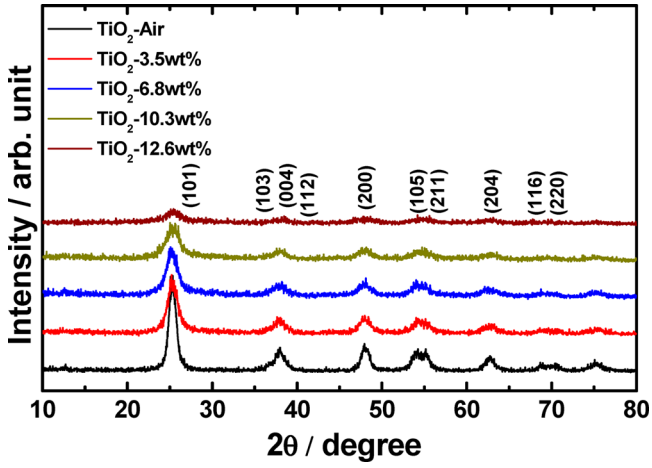

Figure 1. XRD patterns of TiO_2 powders with different amounts of carbon sources.

of sucrose. The resulting XRD patterns were in good agreement with the anatase phase, which has the tetragonal space group with $I41/amd$ (141).[17] Table 1 lists the calculated lattice parameters of each TiO_2 powder. The lattice parameters remained more or less constant regardless of the carbon content (pure TiO_2: a = 3.780(9) Å, c = 9.501(4) Å, V = 135.824 $Å^3$). No secondary phases were founded in any samples; however, the peak intensity decreased substantially with increasing carbon-coating amounts. This behavior is also shown in the previous carbon-coated TiO_2 materials.[18,19] As expected, the overall carbon content in the final calcined TiO_2 powders increased with increasing amounts of added sucrose. The carbon content of each powder after calcination was measured using elemental analyzer (EA) and thermogravmetric anayzer (TGA) which are shown in Table 2 and Figure S1 in the Supporting Information.

To verify the morphology and particle shape of synthesized TiO_2 materials, we performed the SEM analysis, which is

Table 1. Lattice Parameters of TiO_2 Powders with Different Amounts of Carbon Sources

	TiO_2-Air	TiO_2-3.5 wt %	TiO_2-6.8 wt %	TiO_2-10.3 wt %	TiO_2-12.6 wt %
a axis (Å)	3.780(9)	3.781(3)	3.781(1)	3.780(8)	3.782(1)
c axis (Å)	9.501(4)	9.500(8)	9.501(2)	9.501(4)	9.500(6)
volume ($Å^3$)	135.824	135.844	135.836	135.817	135.899

Table 2. Carbon Contents, Surface Area, and Conductivity of TiO_2 Powders with Different Amounts of Carbon Sources

	TiO_2-Air	TiO_2-3.5 wt %	TiO_2-6.8 wt %	TiO_2-10.3 wt %	TiO_2-12.6 wt %
carbon content (wt %)		3.55	6.84	10.33	12.61
surface area ($m^2\ g^{-1}$)	136.45	128.9	127.27	117.09	102.71
conductivity ($S\ cm^{-1}$)	$\sim 1 \times 10^{-12}$ to 1×10^{-7}	1.1×10^{-5}	3.2×10^{-5}	4.1×10^{-5}	4.7×10^{-5}

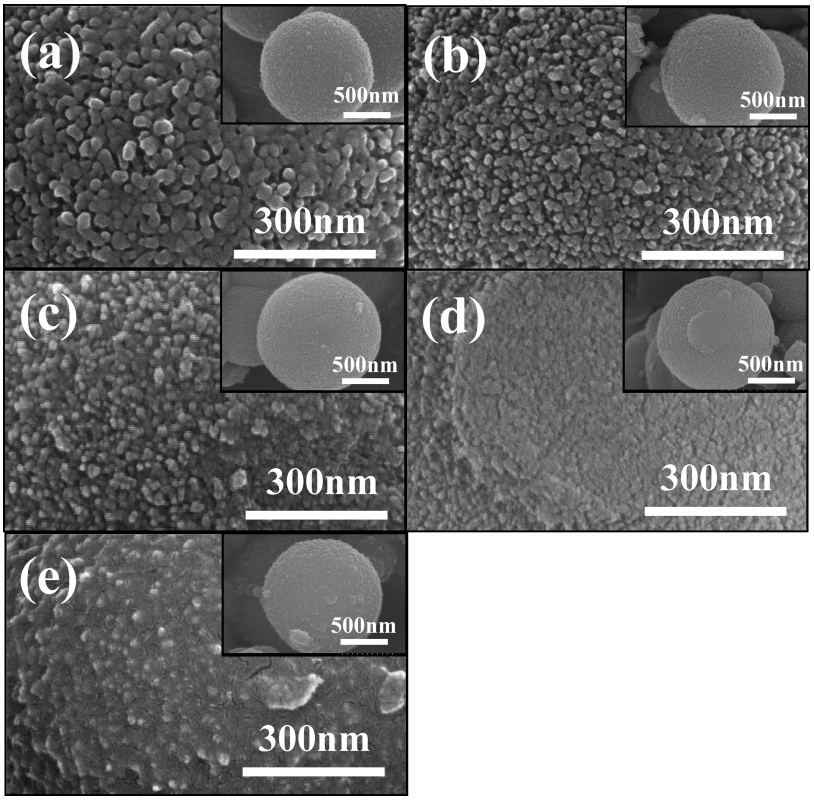

Figure 2. SEM images of TiO_2 powders with different amounts of carbon sources; (a) TiO_2-Air, (b) TiO_2-3.5 wt %, (c) TiO_2-6.8 wt %, (d) TiO_2-10.3 wt %, and (e) TiO_2-12.6 wt %.

presented in Figure 2. As shown in the SEM images, all of the synthesized TiO_2 materials have a micron-sized spherical morphology which consists of nanosized primary crystallites. This TiO_2 materials have high powder tap density of 0.9 g cm^{-3} which is higher than commercialized TiO_2 materials (tap density: 0.13 g cm^{-3}, P25, Degussa, Japan). Through the SEM anlaysis, we observed that the P25-TiO_2 have nanosized morphology which could lead to the low tap density (see Figures S2 and S3 in the Supporting Information). In general, the primary crystallite size increases during calcination because of agglomeration and solid-state sintering. The increased primary crystallite size typically leads to long diffusion length and subsequent deterioration of the electrochemical performance. The previous reports concluded that carbon coating during calcination prevented the agglomeration of primary crystallites and also enhanced the electrical conductivity.[20−22] Figure 2a shows the representative morphology of TiO_2 particles without carbon coating after being calcined in air (hereafter called TiO_2-Air). Compared to the TiO_2-Air material, carbon-coated TiO_2 materials, shown in Figure 2b−e (hereafter called TiO_2-3.5 wt %, TiO_2-6.8 wt %, TiO_2-10.3 wt %, and TiO_2-12.6 wt %), had primary crystallites whose sizes were considerably smaller than those of the noncoated TiO_2. With increasing amounts of carbon, the surface morphology of the TiO_2 particle also substantially changed. Surfaces of TiO_2-10.3 wt % and TiO_2-12.6 wt %, especially, were covered with amorphous material, which is assumed to likely be residual carbon. Through the SEM images analysis, we verified the effect of carbon coating on the particle morphology.

TEM images a and b in in Figure 3 show the primary crystallites of TiO_2-Air material whose sizes ranged from 20 to 30 nm. TiO_2-6.8 wt % had smaller primary crystallites (5−10 nm) than TiO_2-Air, in agreement with the SEM data. We also calculated the crystallite sizes of each TiO_2 powder using Scherrer's equation to confirm the TEM analysis results. As observed by TEM images, carbon coated TiO_2 powders show the smaller crystallite sizes (TiO_2-3.5 wt %, 10.922 nm; 6.8 wt %, 10.012 nm; 10.3 wt %, 9.919 nm; and 12.6 wt %, 9.891 nm)

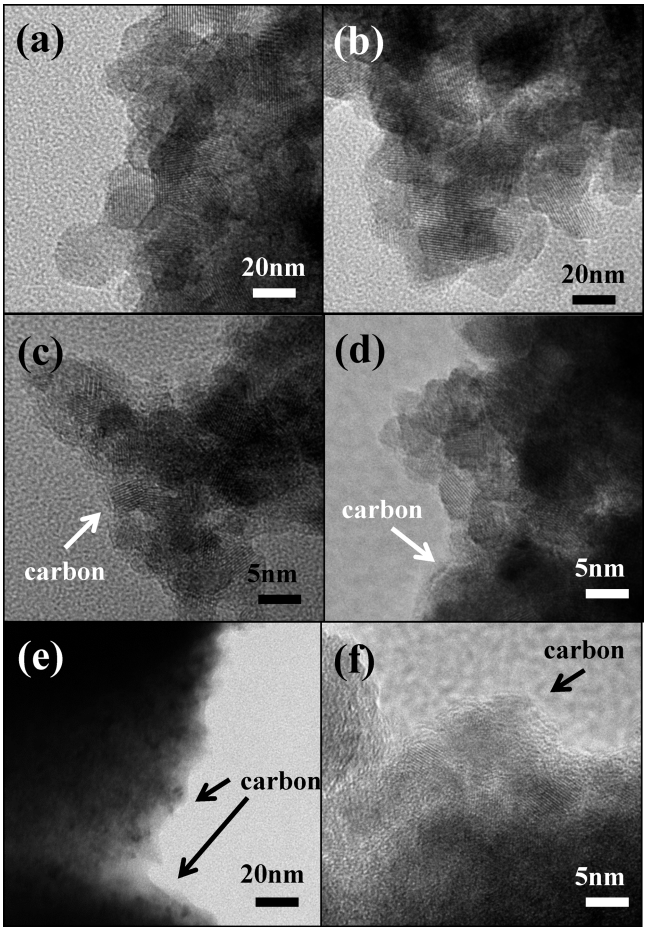

Figure 3. TEM images of (a, b) TiO_2-Air, (c, d) TiO_2-6.8 wt %, (e, f) TiO_2-12.6 wt % powders with arrows indicating the carbon coating film.

than noncoated powder (23.852 nm). In addition, a uniform carbon-coating layer was also observed in Figure 3c, d. From the TEM images, we confirmed that the uniform coating of carbon helped to prevent the agglomeration of primary crystallites of TiO_2 during calcination. Meanwhile, an excessive amount of carbon led to a thick carbon-coating layer (10−20 nm), as shown in Figure 3e, f. In this case, it was difficult to observe the particles, which were completely coated by a thick layer of carbon. From the pore-size distribution (PSD) analysis of each TiO_2 material, we found that the TiO_2-10.3 wt % and TiO_2-12.6 wt % materials show the lower pore volume and surface area than other materials (see Figure S4 in the Supporting Information). Compared to TEM results, we confirmed that these lower values were caused by the excessive amount of thick carbon layer, which block the nanopores in TiO_2 particles.

Figure 4a, b show the first and second charge/discharge curves of Na/TiO_2-Air and Na/C-TiO_2 half-cells with different amounts of carbon. The cells were tested over a voltage range of 0.01 to 2.0 V at a constant current density of a 0.1 *C* rate. Before discussing about the electrochemical properties of the cells, we measured the electrochemical performances of amorphous carbon electrode to clarify the capacity contribution by coated amorphous carbon (see Figure S5 in the Supporting Information). The carbon electrode delivered the capacity of 39.2 mAh g^{-1} at a 0.1 *C* rate with poor cycle and rate performances. And, we calculated the capacity contributions of the amorphous carbon in the carbon-coated TiO_2 electrodes with different amounts of carbon sources (see Table S1 in the Supporting Information). From these results, we confirmed that the capacity contribution by the amorphous carbon is negligible in TiO_2-3.5 wt %, TiO_2-6.8 wt % electrodes. Meanwhile, this amorphous carbon could contributed to the electrochemical performances of TiO_2-10.3 wt %, TiO_2-12.6 wt % electrodes because of higher carbon contents.

The first charge curve was divided into several regions, and each reaction was analyzed based on the previous literature on sodium battery anodes. In the first charge curves of the cyclic voltammogram (CV) profile, shown in Figure 4c, the irreversible peaks were observed which caused by the solid electrolyte interface (SEI) layer formation, irreversible sites for Na-ion insertion in the crystal lattice defects, electrolyte, fluoroethylene carbonate (FEC) additive, and other organic material decomposition.[16,23] We also measured the surface areas of each TiO_2 powder to determine the relationship between surface area and SEI formation. As expected, TiO_2-Air powder showed the largest surface area than carbon coated TiO_2 powders, that means larger amounts of electrolyte could be contact with surface of TiO_2-Air powders. For that reason, TiO_2-Air electrode showed the highest first discharge capacity, which was caused by the side reaction such as SEI formation and electrolyte decomposition. From the second cycle on, TiO_2 electrodes show only the reversible insertion/deinsertion peaks at 0.5 and 0.8 V in the CV profiles. Therefore, it is conjectured that the large irreversible capacity likely originated from electrolyte decomposition and SEI layer formation during the first cycle and disappeared from subsequent cycles. Figure 4d shows the ex situ XRD result of the TiO_2-6.8 wt % electrode at different states of charge/discharge points during the first cycle (each point in Figure 4a, d: a = pristine, b = discharged up to 1.0 V, c = discharged up to 0.01 V, d = charged up to 1.0 V, and e = charged up to 2.0 V). During the first cycle, there were no peak changes in the XRD data during different states of charge and discharge which are well-matched with the previous result. Also, we could not observe the new peaks, such as Ti metal and Na_2O, which indicates the conversion reaction.[16] It is hard to determine the reaction mechanism of the TiO_2-6.8 wt % electrode using XRD analysis. Therefore, other analysis results were needed to understand the reaction mechanism of this electrode. To investigate the variation of an average oxidation state of Ti during cycling, we performed the ex situ X-ray photoelectron spectroscopy (XPS) analysis which shown in Figure 4e. The main peak of TiO_2 pristine (marked a) is 458.2 eV which means average titanium oxidation state is 4+. This peak was gradually shifted into 457.9 eV during the discharge and returned to original value after charge process which means the oxidation state is partially reduced to $Ti^{3+/4+}$ mixed state during the discharge process and recovered to Ti^{4+} after the charge process. From these results, we confirmed the TiO_2 electrode show the reversible insertion/deinsertion reaction during cycling. We also measured the XPS analysis for each TiO_2 powder to determine the possibility of incorporating carbon into a portion of the TiO_2 structure (see Figure S6 in the Supporting Information). However, we could not found any evidence about the oxidation state change of Ti^{4+} after carbon coating.

Cycle performances of TiO_2 half-cells are shown in Figure 5. All cells were discharged up to 0.01 V and charged up to 2.0 V with the constant current of a 0.2 *C* rate at 25 °C. The TiO_2-Air cells show stable cycle performance. The carbon-coated TiO_2-

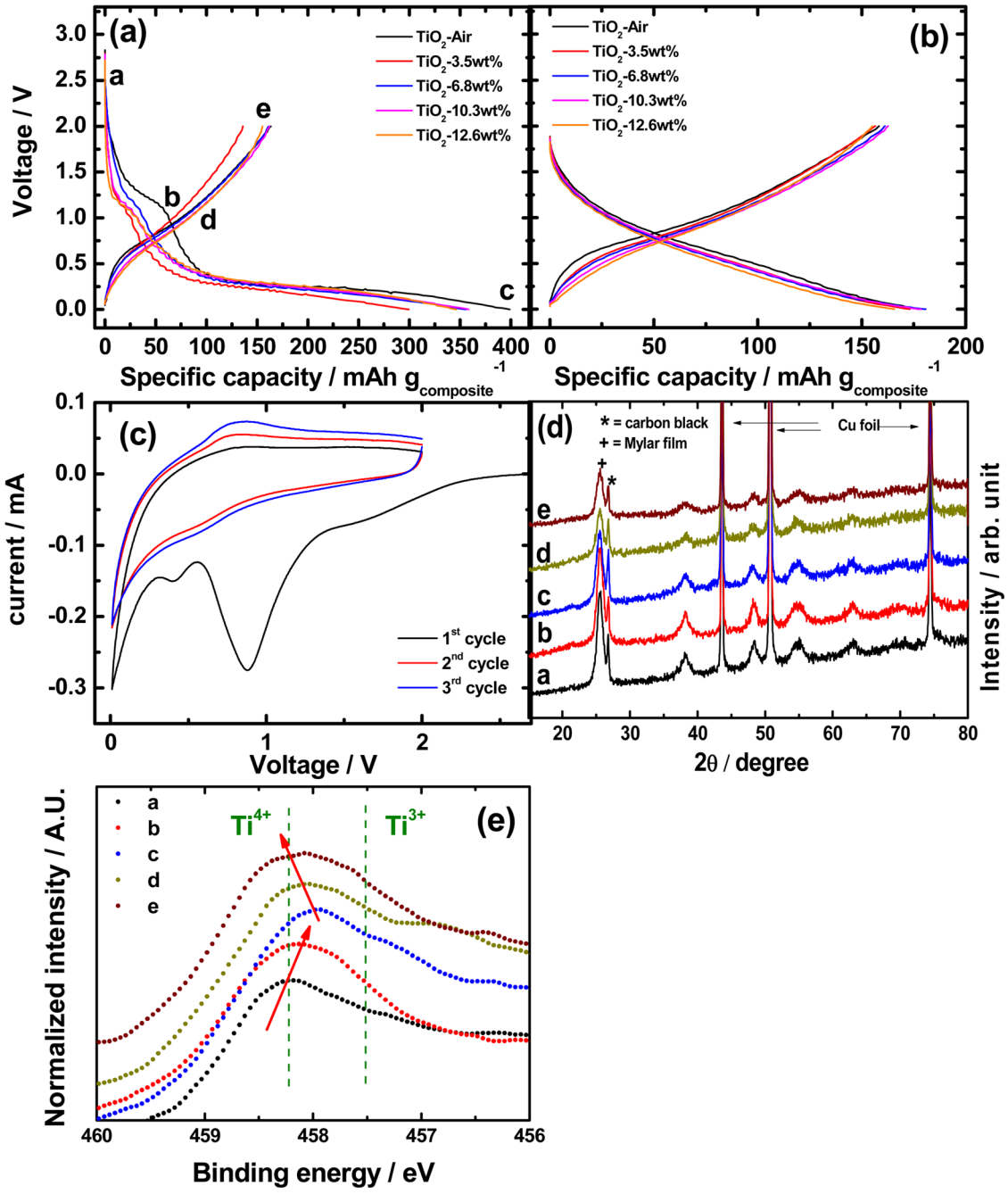

Figure 4. (a) First charge/discharge curves and (b) second cycle curves of Na/TiO_2 cells. Cells were charged at a constant-current 0.1 *C* rate to 0.01 V and discharged at a constant-current 0.1 *C* rate to 2.0 V at 25 °C. (c) Cyclic voltammogram of the Na/TiO_2-6.8 wt % cell, (d) ex situ XRD patterns of TiO_2-6.8 wt % electrode (Mylar film was used for protection of electrode against the air atmosphere), and (e) ex situ X-ray photoelectron spectroscopy (XPS) results of TiO_2 electrode during 1st cycle (each state of charge points are marked in image a: a = pristine, b = discharged up to 1.0 V, c = discharged up to 0.01 V, d = charged up to 1.0 V, and e = charged up to 2.0 V).

3.5 wt % and TiO_2-6.8 wt % cells also show nearly 100% cycle retention during 50 cycles, despite the large irreversible capacity observed during the first cycle. This excellent cycle performance is believed to be due to the morphological advantage of the synthesized material and structural stability of TiO_2 itself. The stable cycle performance also verified in the charge/discharge curves of the TiO_2-6.8 wt % electrode during cycling (Figure 5b). During the cycle test, no voltage drop or curve changes were observed. However, TiO_2-10.3 wt % and TiO_2-12.6 wt % cells show lower cycle retention than other cells. From the SEM and TEM images, we assumed that the large amount of carbon (a thick coating layer) affected the cell performance. The thick carbon coating layer interrupted the Na^+ insertion/deinsertion process and led to the capacity fading during cycling.

Panels a and b in Figure 6 show the rate performance of the TiO_2 cells. All cells were charged up to 0.01 V with the constant current of a 0.1 *C* rate, and discharged up to 2.0 V with the various constant current of 0.1−30 *C* rate (except the TiO_2-Air cell). The carbon-coated TiO_2 electrodes showed better rate capability than the noncoated electrode. The TiO_2-6.8 wt % electrode, in particular, exhibited a good rate capability up to a

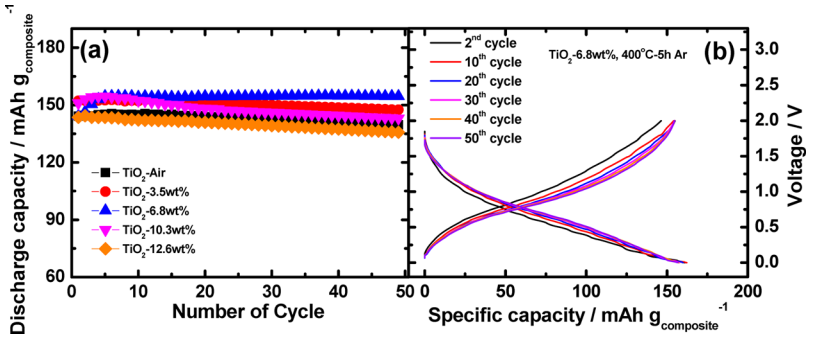

Figure 5. (a) Discharge capacity versus number of cycles for Na/TiO_2 cells at 0.1 *C* rate cycled at 25 °C, and (b) charge/discharge profiles of the Na/TiO_2-6.8 wt % cell during the 50th cycle.

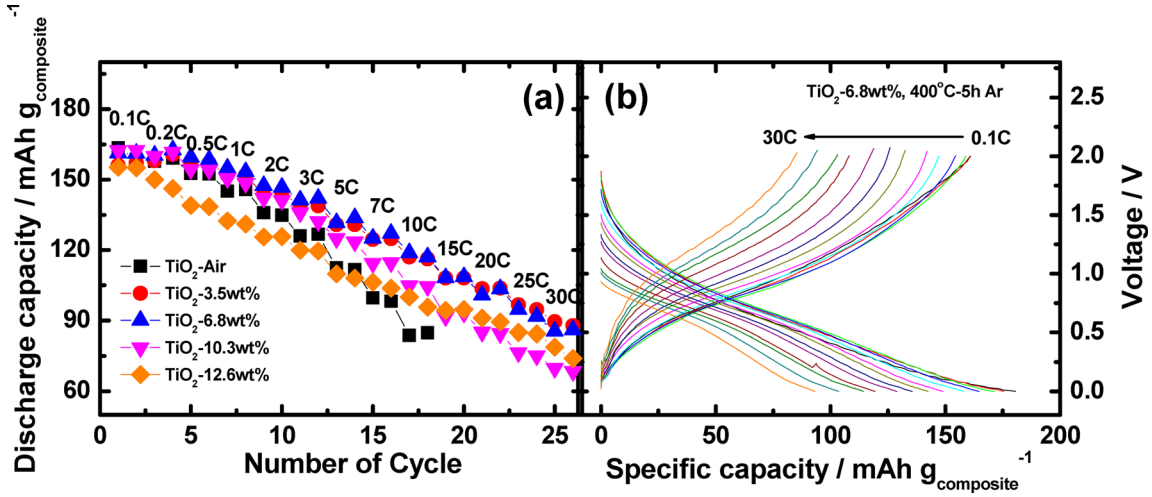

Figure 6. (a) Rate capability of Na/TiO_2 cells and (b) charge/discharge curves of Na/TiO_2-6.8 wt % cell between 0.01 and 2.0 V at 25 °C. The cell was charged with a constant current of a 0.1 *C* rate to 0.01 V and discharged with a constant current of a 0.1−30 *C* rate.

30 *C* rate: 155 mAh $g_{composite}^{-1}$ at 0.1 *C*, 149 mAh $g_{composite}^{-1}$ at 1 *C*, and 82.7 mAh $g_{composite}^{-1}$ at a 10 *C* rate. The improved rate capability of the TiO_2-6.8 wt % electrode partially stemmed from the disparately higher electrical conductivity of the TiO_2-6.8 wt % electrode. Non-carbon-coated TiO_2-Air powder has very low electrical conductivity (~1×10^{-12} to 1×10^{-7} S cm^{-1}),[24] whereas TiO_2-6.8 wt % powder has much higher electrical conductivity of 3.2×10^{-5} S cm^{-1} (Table 2, measured by a four-point DC method). This behavior clearly explains that the small primary crystallites and proper carbon coating layer not only decrease the resistance during the insertion/extraction process, but also increase the electrical conductivity of the material. On the other hand, the non-carbon-coated TiO_2-Air electrode has large primary crystallites compared to the carbon-coated electrodes, and these large primary crystallites likely cause the rapid capacity drop. The charge/discharge curves of the TiO_2-6.8 wt % electrode at different *C* rates are shown in Figure 6b. As the *C* rate increased, the discharge capacity progressively decreased, but with no significant voltage drop during the rate test. The result confirms that the carbon-coated TiO_2-6.8 wt % cell shows superior electrochemical properties.

We could found the trend between carbon contents and electrochemical performance through the electrochemical test of amorphous carbon and morphological analysis (PSD, TEM). From these results, we concluded the rate and cycle properties of C-TiO_2 (TiO_2-10.6 wt %, 12.3 wt %) electrodes were rather decreased than other carbon-coated electrodes, which is caused by the excessive amounts of amorphous carbon (low pore volume and surface area, poor electrochemical properties).

CONCLUSIONS

Carbon-coated microsphere TiO_2 materials with high tap density were successfully synthesized by a hydrothermal method followed by sucrose carbon coating for testing for sodium-ion batteries. We compared the effect of the carbon coating by characterizing the physical and electrochemical properties in the sodium battery system. Although these materials have high tap density and micron particle size, the TiO_2-6.8 wt % electrode exhibited the best cycle performance (100% cycle retention during the fiftieth cycle) and the best rate capability, delivering the discharge capacities of 155 mAh $g_{composite}^{-1}$ at 0.1 *C*, 149 mAh $g_{composite}^{-1}$ at 1 *C*, and 82.7 mAh $g_{composite}^{-1}$ at a 10 *C* rate, respectively. These excellent properties were ascribed to the uniformly coated carbon layer, which prevented the agglomeration of primary crystallites during calcination and greatly increased the electrical conductivity. This superior carbon-coated TiO_2 material should be acceptable as safe and low-cost anode material for sodium-ion batteries with high power capability.

ASSOCIATED CONTENT

Supporting Information

Additional TGA, tap density, BET, SEM, XPS results of C-TiO_2, and electrochemical performances of amorphous carbon.

This material is available free of charge via the Internet at http://pubs.acs.org/.

AUTHOR INFORMATION

Corresponding Author

*E-mail: yksun@hanyang.ac.kr.

Notes

The authors declare no competing financial interest.

ACKNOWLEDGMENTS

This work was supported by the Global Frontier R&D Program (2013-073298) on Center for Hybrid Interface Materials (HIM) funded by the Ministry of Science, ICT & Future Planning. and the Human Resources Development program (20124010203310) of the Korea Institute of Energy Technology Evaluation and Planning (KETEP) grant funded by the Korea government Ministry of Trade, Industry and Energy.

REFERENCES

(1) Scrosati, B. Technology: Charging Towards the Superbattery. *Nature* **2011**, *473*, 448−449.

(2) Scrosati, B.; Hassoun, J.; Sun, Y.-K. Lithium-Ion Batteries − A Look into the Future. *Energy Environ. Sci.* **2011**, *4* (9), 3287−3295.

(3) Stevens, D. A.; Dahn, J. R. High Capapcity Anode Materials for Rechargeable Sodium-Ion Batteries. *J. Electrochem. Soc.* **2000**, *147*, 1271−1273.

(4) Wenzel, S.; Hara, T.; Janek, J.; Adelhelm, P. Room-Temperature Sodium-Ion Batteries: Improving the Rate Capability of Carbon Anode Materials by Templating Strategies. *Energy Environ. Sci.* **2011**, *4*, 3342−3345.

(5) Stevens, D. A.; Dahn, J. R. The Mechanisms of Lithium and Sodium Insertion in Carbon Materials. *J. Electrochem. Soc.* **2001**, *148*, A803−A811.

(6) Thomas, P.; Ghanbaja, J.; Billaud, D. Electrochemical Insertion of Sodium in Pitch-Based Carbon Fibers in Comparison with Graphite in $NaClO_4$-Ethylene Carbonate Electrolyte. *Electrochim. Acta* **1999**, *45*, 423−430.

(7) Komaba, S.; Murata, W.; Ishikawa, T.; Yabuuchi, N.; Ozeki, T.; Nakayama, T.; Ogata, A.; Gotoh, K.; Fujiwara, K. Electrochemical Na Insertion and Solid Electrolyte Interphase for Hard-Carbon Electrodes and Application to Na-Ion Batteries. *Adv. Funct. Mater.* **2011**, *21*, 3859−3867.

(8) Alcantara, R.; Jimenez-Mateos, J. M.; Lavela, P.; Tirado, J. L. Carbon Black: A Promising Electrode Material for Sodium-Ion Batteries. *Electrochem. Commun.* **2001**, *3*, 639−642.

(9) Rudola, A.; Saravanan, K.; Mason, C. W.; Balaya, P. $Na_2Ti_3O_7$: An Intercalation Based Anode for Sodium-Ion Battery Applications. *J. Mater. Chem. A* **2013**, *1*, 2653−2662.

(10) Senguttuvan, P.; Rousse, G.; Seznec, V.; Tarascon, J.-M.; Palacin, M. R. $Na_2Ti_3O_7$: Lowest Voltage ever Reported Oxide Insertion Electrode for Sodium Ion Batteries. *Chem. Mater.* **2011**, *23*, 4109−4111.

(11) Park, S. I.; Gocheva, I.; Okada, S.; Yamaki, J. Electrochemical Properties of $NaTi_2(PO_4)_3$ Anode for Rechargeable Aqueous Sodium-Ion Batteries. *J. Electrochem. Soc.* **2011**, *158*, A1067−A1070.

(12) Komaba, S.; Mikumo, T.; Yabuuchi, N.; Ogata, A.; Yoshida, H.; Yamada, Y. Electrochemical Insertion of Li and Na Ions into Nanocrystalline Fe_3O_4 and α-Fe_2O_3 for Rechargeable Batteries. *J. Electrochem. Soc.* **2010**, *157*, A60−A65.

(13) Xu, Y.; Lotfabad, E. M.; Wang, H.; Farbod, B.; Xu, Z.; Kohandehghan, A.; Mitlin, D. Nanocrystalline Anatase TiO_2: A New Anode Material for Rechargeable Sodium Ion Batteries. *Chem. Commun.* **2013**, *49*, 8973−8975.

(14) Wu, L.; Buchholz, D.; Bresser, D.; Chagas, L. G.; Passerini, S. Anatase TiO_2 Nanoparticles for High Power Sodium-Ion Anodes. *J. Power Sources* **2014**, *251*, 379−385.

(15) Gonzalez, J. R.; Alcantara, R.; Nacimiento, F.; Ortiz, G. F.; Tirado, J. L. Microstructure of the Epitaxial Film of Anatase Nanotubes Obtained at High Voltage and the Mechanism of Its Electrochemical Reaction with Sodium. *CrystEngComm* **2014**, *16*, 4602−4609.

(16) Kim, K.-T.; Ali, G.; Chung, K. Y.; Yoon, C. S.; Yashiro, H.; Sun, Y.-K.; Lu, J.; Amine, K.; Myung, S.-T. Anatase Titania Nanorods as an Intercalation Anode Material for Rechargeable Sodium Batteries. *Nano Lett.* **2014**, *14* (2), 416−422.

(17) Jung, H.-G.; Oh, S. W.; Ce, J.; Jayaprakash, N.; Sun, Y.-K. Mesoporous TiO_2 Nano Networks: Anode for High Power Lithium Battery Applications. *Electrochem. Commun.* **2009**, *11*, 756−759.

(18) Park, S.-J.; Kim, Y.-J; Lee, H. Synthesis of Carbon-Coated TiO_2 Nanotubes for High-Power Lithium-Ion Batteries. *J. Power Sources* **2011**, *196*, 5133−5137.

(19) Park, S.-J.; Kim, H.; Kim, Y.-J.; Lee, H. Preparation of Carbon-Coated TiO_2 Nanostructures for Lithium-Ion Batteries. *Electrochim. Acta* **2011**, *56*, 5355−5362.

(20) Oh, S.-M.; Sun, Y.-K. Improving the Electrochemical Performance of $LiMn_{0.85}Fe_{0.15}PO_4$-$LiFePO_4$ Core-Shell Materials Based on an Investigation of Carbon Source Effect. *J. Power Sources* **2013**, *244*, 663−667.

(21) Jung, H.-G.; Myung, S.-T.; Yoon, C. S.; Son, S.-B.; Oh, K. H.; Amine, K.; Scrosati, B.; Sun, Y.-K. Microscale Spherical Carbon-Coated $Li_4Ti_5O_{12}$ as Ultra High Power Anode Material for Lithium Batteries. *Energy Environ. Sci.* **2011**, *4*, 1345−1351.

(22) Chen, Z.; Dahn, J. R. Reducing Carbon in $LiFePO_4$/C Composite Electrodes to Maximize Specific Energy, Volumetric Energy, and Tap Density. *J. Electrochem. Soc.* **2002**, *149*, A1184−A1189.

(23) Komaba, S.; Ishikawa, T.; Yabuuchi, N.; Murata, W.; Ito, A.; Ohsawa, Y. Fluorinated Ethylene Carbonate as Electrolyte Additive for Rechargeable Na Batteries. *ACS Appl. Mater. Interfaces* **2011**, *3*, 4165−4168.

(24) Wang, W.; Sa, Q.; Chen, J.; Wang, Y.; Jung, H.; Yin, Y. Porous TiO_2/C Nanocomposite Shells as a High-Performance Anode Material for Lithium-Ion Batteries. *ACS Appl. Mater. Interfaces* **2013**, *5*, 6478−6483.